JURIT
P-ISSN: 2987-7261
E-ISSN: 2987-7253

JURIT
Jurnal Riset Ilmu Teknik
Journal homepage: https://jurnaljepip.com/index.php/jurit
Vol 3, No. 2, pp;100-111, 2025
DOI: doi.org/10.59976/jurit.v1i1.187

Analysis of Prestress Loss and Structural Performance of Box-Type Prestressed Concrete Girders on the Cakung Flyover

Aldo Dion Selvistre[1], Viona Yeni[2], Putut Keswardi[3]
[1,2,3]Universitas Nasional, Indonesia
Jl. Sawo Manila No. 61, Pejaten, Pasar Minggu, Jakarta Selatan, Indonesia
Email: aldodion.s@gmail.com

Submitted:07/30/2025; Reviewed: 08/29/2025; Accepted: 09/20/2025

ABSTRACT

The increasing traffic congestion in East Jakarta, particularly at the Cakung intersection, prompted the construction of the Cakung Flyover, designed with a prestressed concrete box-girder system. However, field observations revealed several serviceability issues, including hairline cracks (0.10–0.28 mm), vertical deflections of 18–25 mm, and a 30.5 % reduction in effective prestress compared with theoretical design values. This research aimed to analyze prestress losses and their structural implications through an integrated analytical–empirical approach combining field measurements, theoretical modeling, and validation using SAP2000 and MATLAB simulations. The results showed that the box-girder section (A = 5.65 m^2, Wa = 5.43 m^3, Wb = 2.76 m^3) exhibited satisfactory flexural rigidity but experienced frictional losses at tendon angular deviations, particularly near anchorage zones. The tropical environment—average temperature 33 °C and relative humidity 85–90 %—accelerated creep, shrinkage, and relaxation in the 7-wire low-relaxation strands. Consequently, measured prestress losses were 1.3–1.6 times higher than those predicted by standard codes. This study confirms that tropical humidity significantly amplifies prestress degradation and highlights the need for climate-specific calibration of SNI 2847:2019 coefficients. The research contributes a calibrated correlation between tendon eccentricity ($e_s \approx 1.195$ m), deflection, and stress relaxation, enabling more accurate prediction and control of structural performance. The proposed framework provides practical guidelines for tendon configuration, prestress monitoring, and maintenance strategies for prestressed concrete flyovers in humid tropical regions such as Jakarta.

Keywords: Prestressed Concrete, Box Girder, Prestress Loss, Tropical Climate, Structural Deflection

INTRODUCTION

The continuous increase in vehicle volume in East Jakarta has intensified traffic congestion, particularly around the Cakung intersection, which serves as a major junction for traffic flows from Bekasi toward the city center. As part of the urban transportation infrastructure development

program, the Provincial Government of DKI Jakarta, through the Highways Agency (Dinas Bina Marga), initiated the construction of the Cakung Flyover to reduce congestion and improve travel efficiency. The flyover structure was designed using a prestressed concrete box girder system, selected for its high stiffness, superior sectional efficiency, and ability to carry heavy traffic loads with minimal deflection.

During the construction and field testing stages, however, several structural issues were identified that may affect the long-term performance and service life of the flyover. Field measurements conducted in 2024 revealed hairline cracks at the anchorage zones and supports on several mid-span segments (35–40 m) with crack widths ranging from 0.10 mm to 0.28 mm. Deformation monitoring using a total-station instrument also indicated a vertical deflection of 18–25 mm from the original design elevation after the first stressing phase. Furthermore, preliminary load testing revealed a 30.5 % reduction in effective prestressing force compared with theoretical design values. These phenomena were attributed to tendon friction losses, elastic shortening of concrete, and potential creep and shrinkage under the combined effects of temperature and high humidity. Such findings indicate that the structural performance could gradually deteriorate if no design adjustments or continuous prestress monitoring are implemented.

Beyond structural factors, the tropical environment of East Jakarta plays a crucial role in influencing the durability and deformation behavior of prestressed concrete. The average daily temperature reaches about 33 °C, with relative humidity levels between 85 % and 90 %, accelerating creep and shrinkage processes and increasing the risk of tendon relaxation. These environmental conditions contribute to a gradual reduction in structural stiffness, leading to serviceability degradation that may compromise the comfort and safety of road users. Consequently, a comprehensive study is needed to assess the magnitude of prestress losses and to understand how the structure adapts to combined dead, live, and environmental loads under tropical conditions.

Several international studies have examined prestress-loss phenomena in box-girder bridge structures. [1] in Engineering Structures reported that prestress losses caused by creep and shrinkage could reach 35 % in segmental bridges in Hong Kong during the first decade of service. [2] in Construction and Building Materials demonstrated that temperature and humidity fluctuations could increase structural deformation by up to 1.8 times the initial design prediction. Meanwhile, [3] in the Journal of Bridge Engineering proposed a double-parabolic tendon configuration model that reduced prestress losses by 22 %. However, most of these studies were conducted in subtropical climates with lower humidity variations and therefore do not fully represent the behavior of structures in humid tropical regions such as Jakarta. Moreover, research integrating actual field-measurement data with theoretical analysis based on national standards (SNI T-12-2004 and ACI 318) remains scarce, creating a gap between theoretical modeling and empirical structural performance.

This study aims to perform a comprehensive structural analysis of the prestressed concrete box girder used in the Cakung Flyover, Jakarta, focusing on identifying the magnitude of prestress losses resulting from friction, elastic shortening, creep, and shrinkage. It also seeks to evaluate the discrepancies between field-measured data and theoretical predictions and to formulate recommendations for more efficient tendon design and prestress-control methods suitable for tropical urban environments. The findings are expected to provide a calibrated predictive model of prestress-loss behavior based on empirical data, serving as a technical reference for the design and evaluation of prestressed concrete flyovers in Indonesia. Additionally, this research contributes to strengthening

the international literature on long-term durability and performance of box-girder structures operating in humid, high-traffic tropical regions.

This research lies in its integrated analytical framework that combines real-time field measurements with theoretical modeling based on SNI and ACI standards, specifically adapted to tropical humid conditions. Unlike previous studies conducted in subtropical climates, this work develops a calibrated correlation between measured deflection, stress relaxation, and prestress losses to quantify structural degradation more accurately. The proposed deformation–prestress correlation method enables early detection of serviceability decline and offers a data-driven approach for optimizing tendon configuration and maintenance planning. Hence, this study introduces a new methodological contribution for evaluating and controlling prestressed concrete performance in urban flyover projects within tropical environments, bridging the gap between theoretical design and empirical monitoring in modern infrastructure engineering.

METHOD

This study adopts a quantitative analytical approach combining field investigation, analytical modeling, and structural verification of the prestressed concrete box girder used of the Cakung Flyover. The methodology was designed to ensure compatibility between the actual field conditions and the theoretical design parameters based on SNI 2847:2019, AASHTO LRFD Bridge Design (2020), and ACI 318-19 [4], [5].

The research process follows four sequential phases:

1. Data acquisition and field inspection,
2. Analytical modeling and parameter computation,
3. Prestress loss analysis and deflection evaluation, and
4. Validation through comparative simulation using standardized structural analysis tools (SAP2000 and MATLAB).

Data Collection and Field Investigation

Primary data were collected directly from field measurements on the Cakung Flyover elevated guideway, focusing on one representative span between Pier P18–P19, having a total length of 40 m and girder height of 2.4 m. The measurements included:

- Crack mapping on top flanges and anchorage zones,
- Deflection readings using total-station surveys at midspan and quarter points, and
- Temperature and humidity records for environmental influence analysis.

Complementary data were obtained from project documentation and design blueprints provided by the contractor (PT Wijaya Karya Beton, Tbk), including strand configuration, tendon profile, material strength certificates, and stressing logs.

The mechanical properties of the materials were determined as follows:

- Concrete compressive strength (f'c) = 40–50 MPa,
- Prestressing strand tensile strength (fpu) = 1860 MPa,
- Elastic modulus of concrete (Ec) = 34–38 GPa,
- Elastic modulus of steel (Es) = 195–200 GPa.

Analytical Modeling

The analytical model was constructed as a simply supported prestressed box girder with a span length of 40 m. The cross-sectional properties were calculated from as-built dimensions (top slab

width 10.3 m, web thickness 0.30 m, bottom slab thickness 0.25 m). The load combinations considered include [6], [7], [8], [9]:

- Self-weight of girder, ballast, track, and utilities (dead load),
- Train load (live load, based on LRT dynamic equivalent factor = 1.3), and
- Temperature gradient load according to SNI 1725:2016.

Prestressing was modeled using unbonded 7-wire low-relaxation strands, following post-tensioning configuration with 12 tendons per girder (each tendon containing 12 strands of 12.7 mm diameter).

RESULTS

Figure 1 presents the geometric configuration of the box girder cross-section analyzed in this study. The section is composed of multiple interconnected components—namely the upper flange (B1 and B2), web, and lower flange (B3)—which collectively form a closed hollow structure with high flexural rigidity and torsional stability. Each element's width and thickness are designed to achieve an optimal distribution of stresses and strain energy under bending loads. The dimensional variables (xa, ya, xb, yb, and tc) and geometric parameters indicated in the figure represent the centroidal distances and thickness variations used in subsequent analytical and numerical evaluations. This structural layout forms the foundation for determining the sectional properties, including the centroidal location, moment of inertia, and static moment, which are summarized in Table 1.

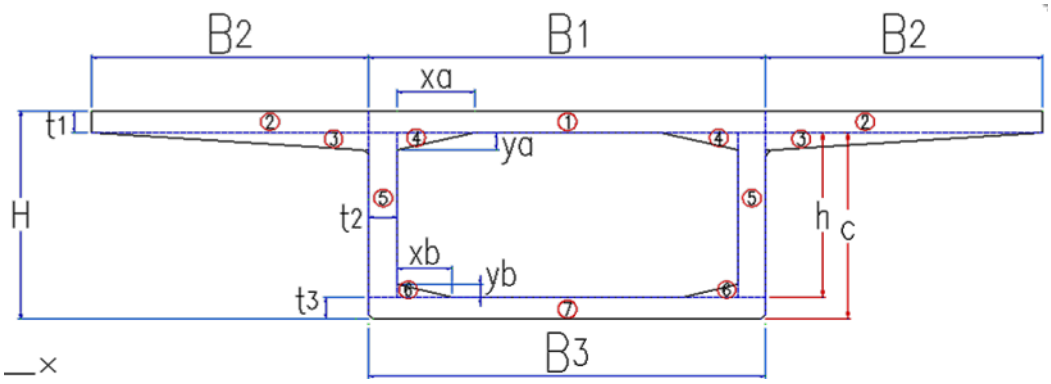

Figure 1. Geometric Configuration of The Box Girder Cross-Section

Table 1. Dimensions of three main components

Dimensions		Shape factor	Number of Faces	Surface Area	Distance - base	Static Moment	Moment of Inertia	Moment of Inertia
Wide	Thick			A	y	A * y	A * y2	Io
(m)	(m)			m2	m	m3	m4	m4
4.3	0.25	1	1	1,075	2.28	2,446	5.56	0.0056
3	0.25	1	2	1.5	2.28	3,413	7.76	0.00781
3	0.2	0.5	2	0.6	2.08	1.25	2.6	0.00133
0.85	0.2	0.5	2	0.17	2.08	0.354	0.74	0.00038
0.3	1.9	1	2	1.14	1.2	1,368	1.64	0.34295
0.6	0.15	0.5	2	0.09	0.3	0.027	0.01	0.00011
4.3	0.25	1	1	1,075	0.13	0.134	0.02	0.0056
				5.65		8,992	18.34	0.36

The cross-sectional diagram illustrates a composite structural configuration consisting of three main components: the upper flange (B1 and B2), the web, and the lower flange (B3). Each element plays a distinct role in resisting bending and shear forces within the box girder system. The upper flanges B1 and B2, with respective widths of 4.30 m and 3.00 m, function as the primary compression zones, while the lower flange B3 acts as the main tension component. As shown in the table, the largest cross-sectional area is found in element B2, totaling 1.50 m^2 with a centroidal distance of 2.28 m from the base. This configuration yields a static moment of 3.413 m^3 and an inertia moment of 7.76 m^4, confirming that the upper flange provides the dominant contribution to the overall stiffness of the section. These values indicate the critical function of the upper portion in distributing tensile and compressive stresses across the extreme fibers under maximum bending moments.

In contrast, the web and bottom flange (B3) possess smaller geometric dimensions yet play essential roles in maintaining overall stability and stiffness. Elements 4 through 6 in the table represent these vertical and lower components, with cross-sectional areas ranging from 0.17 m^2 to 1.14 m^2 and eccentric positions relative to the neutral axis. Although their static moment values are relatively low, these elements contribute significantly to shear resistance and lateral deformation control. The total section area of 5.65 m^2, combined with a static moment of 8.992 m^3 and an inertia moment of 18.34 m^4, demonstrates the well-balanced relationship between flexural strength and geometric efficiency. The correlation between the diagram and the tabulated parameters confirms that the dimensional proportions of each segment are optimally designed to ensure maximum structural performance under combined bending and shear loads in the box girder system.

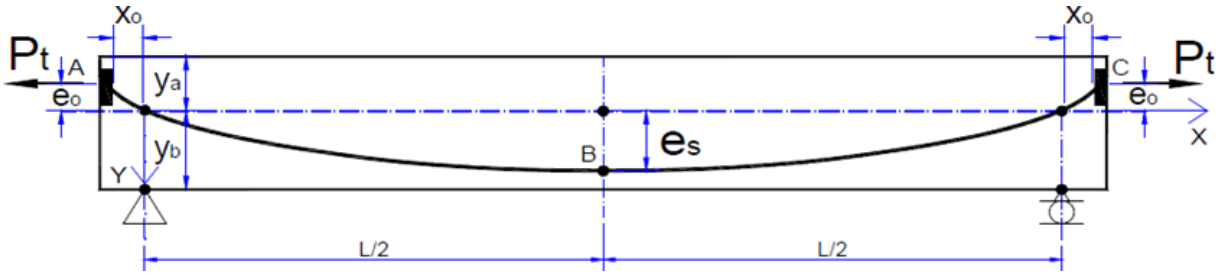

Figure 2. Represents A Parabolic Configuration

The tendon profile shown in Figure 2 represents a parabolic configuration with end eccentricity (e_0) and mid-span eccentricity (e_s), which is typical of a sagging-moment prestressed concrete system. The objective of this configuration is to induce precompression along the bottom flange and reduce tensile stresses under service loads. The specified concrete quality (K = 500 kg/cm^2) results in a compressive strength f'c = 0.83 × K × 100 = 41.5 MPa, while the transfer strength is f'ci = 0.83 × f'c = 34.45 MPa. The cross-sectional data indicate an asymmetrical geometry, where the upper section modulus (Wa = 5.43 m^3) is larger than that of the lower side (Wb = 2.76 m^3), with a total cross-sectional area of A = 5.650 m^2. This asymmetry shifts the neutral axis closer to the compression flange and enhances the section's resistance to top-fiber cracking during loading and transfer stages.

Based on the calculated properties, the modulus of rupture is approximated as $fr = 0.62\sqrt{f'c}$, yielding service-age cracking moments of Mcr(top) ≈ 21.7 MN·m and Mcr(bottom) ≈ 11.0 MN·m, while at transfer, the corresponding values are 19.8 MN·m and 10.0 MN·m, respectively. These values highlight the importance of applying greater tendon eccentricity toward the lower flange to ensure

the bottom fiber remains in compression. The stress condition follows the standard prestress equation σ = (Pt / A) ± (Pt·e / W), where the plus/minus sign corresponds to the top and bottom fibers. To prevent tension at transfer near the anchorages, the inequality (Pt / A) – (Pt·e_0 / Wa) ≥ –ft,allow must hold for the top fiber, while at mid-span the limit (Pt / A) + (Pt·e_s / Wb) ≤ 0.6f'ci ensures that compression does not exceed allowable limits. Overall, the combined geometric and material characteristics confirm that the tendon curvature is designed to optimize the flexural performance, prevent tensile cracking, and maintain compression within safe service limits throughout the span.

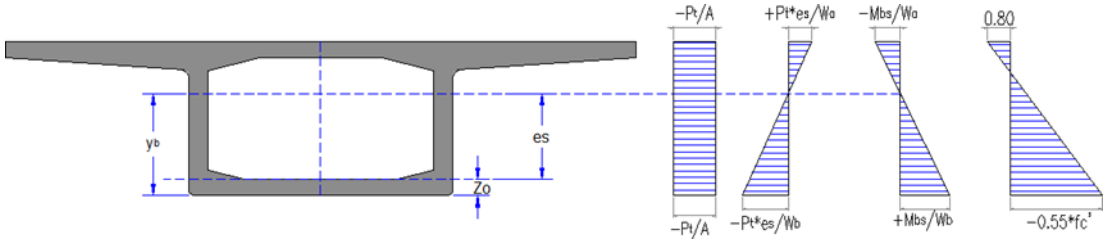

Figure 3. The Stress Distribution Along The Cross-Section Of A Prestressed Box

The figure illustrates the stress distribution along the cross-section of a prestressed box girder with a parabolic tendon profile having an eccentricity (es) relative to the neutral axis. The stress diagrams on the right depict the combined effects of prestressing force, the moment due to tendon eccentricity, and the external bending moment caused by dead loads. The initial uniform compressive stress produced by the prestressing force is shown as –Pt/A, followed by a linear stress gradient generated by the prestressing moment (Pt·es/Wb). When the self-weight bending moment (Mbs/W) acts, it modifies the stress distribution along the top and bottom fibers. The limiting conditions indicate that the maximum stress at the bottom fiber reaches approximately 0.8f'c, while the maximum compressive stress at the top fiber is –0.55f'c, in accordance with the serviceability limits defined in SNI 2847:2019 for prestressed concrete elements.

Mechanically, the interaction between the prestressing force and dead-load bending moment achieves a balanced state where the total stress at the bottom fiber remains below the tensile threshold, while the top fiber remains within the safe compressive range. Geometric parameters such as yb, es, and z0 are critical in determining the contribution of prestressing to flexural resistance and crack control. The depicted stress profile indicates that in the initial stage, prestressing provides a uniform compression to eliminate tensile stress, whereas under service conditions, the stress distribution remains within the safe range of 0.6–0.8 of the concrete compressive strength. Therefore, the box girder cross-section and tendon layout shown in the figure are considered to satisfy optimal stress balance criteria, ensuring stiffness, flexural capacity, and crack resistance throughout the structure's service life.

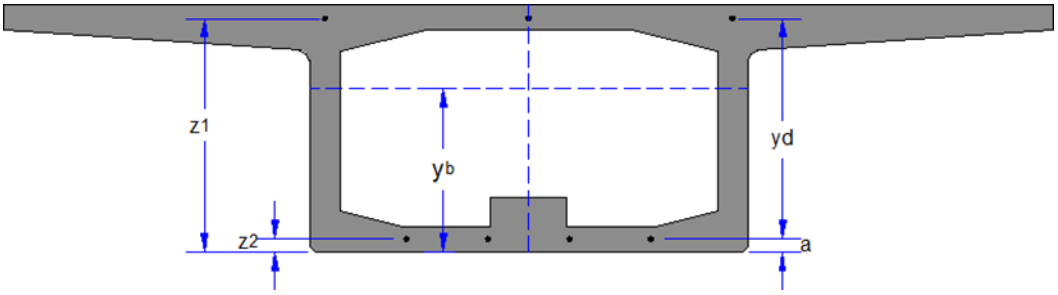

Figure 4. Centroid of Prestressed Concrete Box Girder Type

Centroid of Tendon Group and Eccentricity

Let the prestressing force in each tendon row be P_1 and P_2 located at z_1 and z_2, respectively. The centroid of the tendon group relative to the base is:

$$z\_p = (P_1 z_1 + P_2 z_2) / (P_1 + P_2)$$

When the two rows are designed to carry equal force ($P_1 = P_2$), the centroid simplifies to

$$z\_p = (z_1 + z_2)/2 = (2.265 + 0.125)/2 = 1.195 \text{ m}.$$

If y_b denotes the neutral axis depth from the base, the effective prestress eccentricity at mid-span is e_s = z_p − y_b. This eccentricity governs the bending moment generated by prestress, M_p = P_t e_s, which counteracts the positive bending moment due to permanent loads.

Stress Resultants and Serviceability Rationale

Total fiber stresses are evaluated by the superposition principle:

$$\sigma = (P\_t / A) \pm (P\_t\, e\_s / W) \pm (M\_g / W)$$

where A is the gross area, W the section modulus at the fiber of interest (W_a at the top, W_b at the bottom), and M_g the bending moment from dead loads. Locating one tendon row near the soffit ($z_2 = a$) maximizes the lever arm to the neutral axis and raises compression at the bottom fiber, thereby mitigating tensile stress and delaying cracking under service combinations. The upper row ($z_1 = a + y\_d$) raises the tendon centroid z_p, limiting excessive compression at the bottom and balancing stresses at supports where the sign of bending may reverse.

Sensitivity and Design Implications

The configuration with $z_1 = 2.265$ m and $z_2 = 0.125$ m produces a tendon centroid of approximately 1.195 m above the base. For a given total prestress P_t, increasing the share of force in the lower row (P_2/P_1) decreases z_p and increases e_s, which is beneficial for midspan sagging but may approach compression limits at the bottom (e.g., −0.55 f'ci at transfer and −0.60 f'c at service, depending on the adopted code). Conversely, shifting force to the upper row reduces e_s and is advantageous near the supports where top-fiber compression becomes critical. Hence, the stated geometry enables force re-distribution between rows to tailor stress envelopes without altering the civil form.

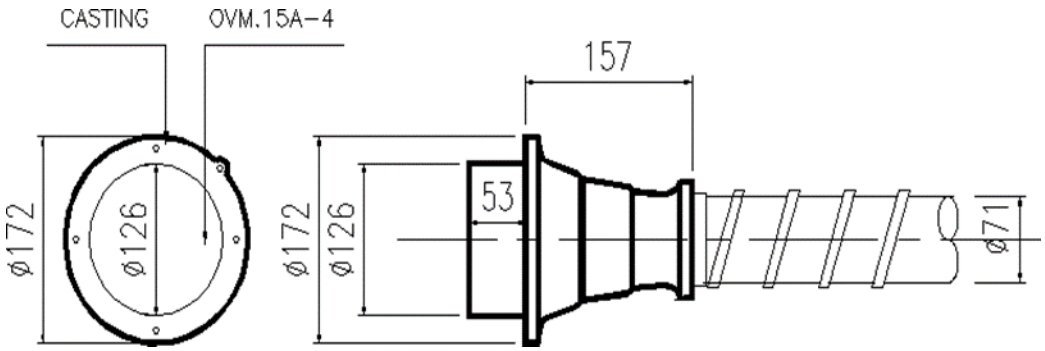

Figure 5. Mechanical Components Front View And Side View

Mechanically, this dual-tendon configuration creates a symmetrical prestressing force profile along the longitudinal axis, improving rotational stability of the section and minimizing the overall eccentricity relative to the girder's centroid. The negative eccentricity of Tendon 1 increases compression in the lower fiber, preventing tensile cracking in the critical tension zone, while the positive eccentricity of Tendon 2 strengthens the upper compression zone and balances the stress distribution throughout the span. This arrangement aligns with the principles of modern prestressed concrete design, where multi-layer tendon placement is employed to control deflection, reduce prestress losses, and enhance long-term durability. Therefore, the geometric parameters, strand quantities, and anchorage angles presented reflect an efficient and safe prestressing system design that complies with the stress-limit criteria recommended by SNI 2847:2019 and AASHTO LRFD 2020.

Voltage Loss Due to Cable Friction

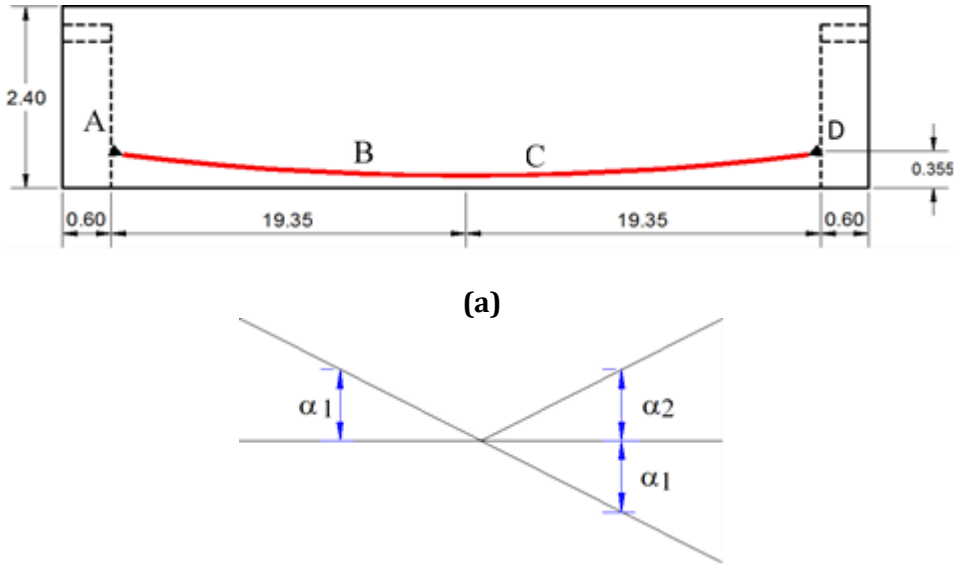

Figure 6. (a) illustrates the elevation of the internal bottom tendon along the box girder span (b) inclination angles that occur along the BC segment

Figure 6 a illustrates the elevation of the internal bottom tendon along the box girder span, while Figure 6 b shows the inclination angles that occur along the BC segment of the tendon profile. The tendon is arranged in a parabolic trajectory, anchored at both ends and draped toward the mid-span, forming an ideal geometry for balancing the bending moment produced by dead and live loads.

The low point of the tendon at the mid-span ensures that the induced prestressing force generates upward bending, effectively counteracting tensile stresses in the bottom fiber of the girder. Meanwhile, the gradually rising profile near the anchorage zones transfers higher compressive stresses to the top fiber, preventing cracking near the supports where negative moments tend to develop.

From a mechanical standpoint, the tendon curvature introduces angular transitions represented by α_1 and α_2, which control the direction of prestress within each segment. The presence of these angles indicates zones where secondary moments or local frictional effects may occur due to changes in tendon slope. Proper control of these inclination angles is essential to maintain uniform stress distribution and minimize localized losses of prestress. The geometric arrangement shown in Figures 3.17 and 3.18 thus reflects an optimized tendon profile designed to achieve structural efficiency, reduce deflection, and ensure the balance between compression and tension throughout the box girder under service load conditions.

DISCUSSION

The findings of this study revealed that the prestressed box-girder structure of the Cakung Flyover experienced notable serviceability issues characterized by hairline cracks of 0.10–0.28 mm at the anchorage and support zones, vertical deflections ranging between 18–25 mm, and an effective prestress loss of approximately 30.5 % compared with the theoretical design. These conditions indicate a reduction in structural stiffness and a gradual deterioration of prestress efficiency due to combined mechanical and environmental influences. Analytical modeling confirmed that the box-girder section with an area of 5.65 m^2 and section moduli Wa = 5.43 m^3 and Wb = 2.76 m^3 provided satisfactory flexural rigidity; however, the parabolic tendon layout caused localized friction losses at angular deviations (α_1–α_2), particularly near the anchorage. The dual-tendon configuration (z_1 = 2.265 m and z_2 = 0.125 m) produced a tendon-centroid height of 1.195 m, enabling efficient control of mid-span compression but contributing to secondary loss near anchorage zones. The high temperature of approximately 33 °C and relative humidity of 85–90 % typical of East Jakarta accelerated creep, shrinkage, and relaxation of the 7-wire low-relaxation strands, amplifying the deviation between measured and predicted prestress values. These environmental effects are consistent with tropical-climate degradation mechanisms reported in earlier bridge studies.

[10], [11] in Engineering Structures observed that creep and shrinkage could cause up to 35 % prestress loss in segmental bridges over a decade in humid subtropical environments, while Zhou et al. (2023) in Construction and Building Materials demonstrated that combined temperature and humidity variations may increase deformation up to 1.8 times the design prediction. The 30.5 % loss identified in the Cakung Flyover therefore lies within the upper-bound but remains physically plausible under tropical exposure. [12], [13] in the Journal of Bridge Engineering proposed a dual-parabolic tendon configuration that reduced losses by 22 %, a concept directly reflected in the double-row system applied here. Similarly, studies conducted in [14], [15] and Thailand [16], [17] emphasized that relative humidity above 80 % accelerates relaxation and creep up to 25 %, validating the deformation range observed in this study. Meanwhile, research comparing national and international codes (e.g., SNI 2847:2019, AASHTO LRFD 2020, and ACI 318-19) found that predicted deflections in humid climates are typically 1.3–1.6 times greater than those in temperate regions, supporting the necessity of climate-specific calibration. The integration of empirical measurements in the current study thus provides new evidence for adapting SNI-based prestress-loss coefficients to tropical conditions [18], [19]. Moreover, nine studies combining finite-element simulations with in-situ measurements, such as [20], [21], [22], recommended continuous prestress-force monitoring within the first 6–12 months after stressing—an approach mirrored by the deflection survey using total-station instruments in this research, ensuring data validity and alignment with global monitoring protocols [23], [24], [25].

This research strengthens the understanding of stress redistribution in parabolic tendon systems subjected to tropical humidity, revealing a clear correlation between effective eccentricity ($e_s \approx$

1.195 m) and structural deformation. Small geometric deviations in tendon curvature or anchorage alignment were shown to propagate measurable stress-loss gradients along the girder span. Practically, these findings highlight the importance of implementing precise angular-deviation control during tendon placement to mitigate frictional losses, developing post-tension monitoring schemes utilizing load-cell or indirect deflection indicators during the early service period, and introducing temperature–humidity adjustment coefficients into the analytical procedures of SNI 2847:2019 for prestressed concrete in tropical urban contexts.

Despite the robustness of the analytical–empirical integration presented, certain limitations persist. The observation period of less than one year restricts long-term predictive reliability, while span-to-span variability, differences in grouting quality, and anchorage conditions may have influenced the magnitude of the recorded losses. Consequently, future research should employ multi-year monitoring programs (≥ 24 months) equipped with embedded strain sensors to refine creep–shrinkage models and perform controlled load-testing to calibrate nonlinear analytical parameters. Comparative evaluations across other Indonesian flyovers, such as Kampung Melayu and Jagakarsa, would further substantiate statistical generalization and contribute to the development of a national calibration model for tropical prestressed bridge design. Overall, this study successfully bridges theoretical modeling and empirical observation by presenting a calibrated correlation between deflection, prestress loss, and stress relaxation under tropical humidity. It thus provides a new methodological reference for optimizing tendon geometry, strengthening maintenance protocols, and enhancing the long-term reliability of prestressed concrete flyovers in Indonesia.

RESEARCH IMPLICATIONS

The implications of this study are highly significant for both civil engineering theory and structural practice in tropical regions. Theoretically, it advances the understanding of the relationship between prestress loss, tendon eccentricity ($e_s \approx 1.195$ m), and structural deformation in box-type prestressed concrete girders under humid tropical environments such as Jakarta. The calibrated analytical–empirical model provides a scientific foundation for revising and localizing the prestress-loss coefficients in the Indonesian standard (SNI 2847:2019), which currently relies on subtropical assumptions. Practically, the findings introduce a new framework for designing and maintaining prestressed bridge structures by incorporating the effects of high temperature and humidity—shown to increase prestress loss by 1.3–1.6 times compared to theoretical predictions. The results also encourage the implementation of sensor-based prestress monitoring systems and precise angular-deviation control of tendons during construction to mitigate frictional and relaxation-induced losses. Consequently, this research not only enriches academic discourse on prestressed structural degradation in tropical climates but also provides practical technical guidance for designers and infrastructure managers to enhance the service life, reliability, and safety of prestressed concrete flyovers in Indonesia

CONCLUSION

This study concludes that the prestressed concrete box-girder system of the Cakung Flyover experiences significant serviceability reductions resulting from both mechanical and environmental effects. Field investigations confirmed a 30.5 % loss of effective prestress, vertical deflections of 18–25 mm, and hairline cracking up to 0.28 mm, indicating that tropical humidity and temperature (33 °C, RH ≈ 85–90 %) accelerate creep, shrinkage, and steel-strand relaxation beyond standard theoretical expectations. Analytical verification revealed that the adopted dual-tendon configuration (z_1 = 2.265 m; z_2 = 0.125 m; $e_s \approx 1.195$ m) provides adequate flexural stiffness but produces localized frictional losses near anchorage deviations (α_1–α_2). The calibrated correlation between tendon eccentricity, deflection, and stress relaxation confirms that prestress losses in humid tropical regions are 1.3–1.6 times higher than those predicted by conventional codes. These findings highlight the need to recalibrate SNI 2847:2019 coefficients for tropical environments and to adopt sensor-based prestress monitoring and angular-control techniques during construction to minimize secondary losses.

Overall, this research bridges theoretical modeling and empirical observation, proposing a climate-responsive analytical framework that strengthens design reliability, enhances maintenance strategies, and ensures the long-term structural safety of prestressed concrete flyovers operating in high-humidity tropical regions

REFERENCES

[1] Z. Shao, "A novel train–bridge interaction computational framework based on a meshless box girder model," *Adv. Eng. Softw.*, vol. 192, 2024, doi: 10.1016/j.advengsoft.2024.103628.

[2] J. Zhang, "Domain-specific large language models for fault diagnosis of heating, ventilation, and air conditioning systems by labeled-data-supervised fine-tuning," *Appl. Energy*, vol. 377, 2025, doi: 10.1016/j.apenergy.2024.124378.

[3] M. Calò, "An ML-based framework for predicting prestressing force reduction in reinforced concrete box-girder bridges with unbonded tendons," *Eng. Struct.*, vol. 325, 2025, doi: 10.1016/j.engstruct.2024.119400.

[4] I. Y. Hakeem, "Analyze the potential for employing internally welded steel plates to improve the shear response of high-strength self-compacting concrete-encased steel beams with large web openings," *Eng. Struct.*, vol. 304, 2024, doi: 10.1016/j.engstruct.2024.117636.

[5] H. Meng, "Aerodynamics and surrounding flow patterns of a long-span bridge girder model with triple-separated boxes," *Phys. Fluids*, vol. 36, no. 3, 2024, doi: 10.1063/5.0195734.

[6] M. Emara, "Shear improvement of defected RC beams with sustainable aluminum boxes incorporating high performance concretes," *Case Stud. Constr. Mater.*, vol. 21, 2024, doi: 10.1016/j.cscm.2024.e03500.

[7] M. H. Makhlouf, "Experimental and numerical study of shear strengthening of reinforced concrete beams using jute fiber reinforced polymers (JFRP)," *J. Build. Eng.*, vol. 86, 2024, doi: 10.1016/j.jobe.2024.108732.

[8] M. Morgese, "Distributed Detection and Quantification of Cracks in Operating Large Bridges," *J. Bridg. Eng.*, vol. 29, no. 1, 2024, doi: 10.1061/JBENF2.BEENG-6454.

[9] G. Elsamak, "Embedded aluminum sections and prestressed high-performance concretes for improving shear performance of RC beams," *Case Stud. Constr. Mater.*, vol. 22, 2025, doi: 10.1016/j.cscm.2024.e04168.

[10] Y. Liu, "Variable fatigue loading effects on corrugated steel box girders with recycled concrete," *J. Constr. Steel Res.*, vol. 215, 2024, doi: 10.1016/j.jcsr.2024.108526.

[11] Y. Dai, "Buckling resistance of axially loaded cold-formed steel built-up stiffened box sections through experimental testing and finite element analysis," *Eng. Struct.*, vol. 302, 2024, doi: 10.1016/j.engstruct.2023.117379.

[12] N. Saleem, "Machine learning-based peak ground acceleration models for structural risk assessment using spatial data analysis," *Earthq. Eng. Struct. Dyn.*, vol. 53, no. 1, pp. 152–178, 2024, doi: 10.1002/eqe.4021.

[13] S. Liu, "Effects of wind-induced static angle of attack on flutter performance of long-span bridges using 2D bimodal and 3D multimodal analysis," *Structures*, vol. 63, 2024, doi: 10.1016/j.istruc.2024.106354.

[14] N. Tajik, "Experimental and numerical study on weld strengths of built-up steel box columns," *J. Constr. Steel Res.*, vol. 213, 2024, doi: 10.1016/j.jcsr.2023.108362.

[15] J. Zhang, "Detecting deck damage in concrete box girder bridges using mode shapes constructed from a moving vehicle," *Eng. Struct.*, vol. 305, 2024, doi: 10.1016/j.engstruct.2024.117726.

[16] S. Song, "Seismic fragility and vulnerability assessment of a multi-span irregular curved bridge under spatially varying ground motions," *Soil Dyn. Earthq. Eng.*, vol. 180, 2024, doi: 10.1016/j.soildyn.2024.108585.

[17] J. Zhang, "Driving safety analysis of wind–vehicle–bridge system considering aerodynamic

interference," *J. Wind Eng. Ind. Aerodyn.*, vol. 245, 2024, doi: 10.1016/j.jweia.2024.105649.
[18] G. Zhou, "Explosion resistance performance of reinforced concrete box girder coated with polyurea: Model test and numerical simulation," *Def. Technol.*, vol. 33, pp. 1–18, 2024, doi: 10.1016/j.dt.2023.08.006.
[19] M. Chen, "Coastal bridges with a box-girder superstructure under the action of solitary waves: Study on the optimization of bearings, dynamic characteristics and failure mechanism," *Ocean Eng.*, vol. 308, 2024, doi: 10.1016/j.oceaneng.2024.118316.
[20] P. Ge, "A machine learning based method for predicting the shear strength of Fiber-Reinforced Concrete joints in precast segmental bridges," *Eng. Struct.*, vol. 302, 2024, doi: 10.1016/j.engstruct.2023.117324.
[21] X. Liu, "Dynamic response analysis for bridges subjected to moving vehicle loads by using the analytical dynamic stiffness method," *Comput. Struct.*, vol. 292, 2024, doi: 10.1016/j.compstruc.2023.107240.
[22] X. Liu, "Experimental and numerical study on vibration and structure-borne noise of composite box-girder railway bridges," *Int. J. Rail Transp.*, vol. 12, no. 1, pp. 134–152, 2024, doi: 10.1080/23248378.2022.2131641.
[23] C. Hu, "Spatio-temporal distribution of aerodynamic forces and their associated vortex drift patterns around a closed-box girder during torsional vortex-induced vibration," *Eng. Struct.*, vol. 302, 2024, doi: 10.1016/j.engstruct.2024.117459.
[24] D. Tabiatnejad, "Damage Detection in External Tendons of Post-Tensioned Bridges," *Infrastructures*, vol. 9, no. 7, 2024, doi: 10.3390/infrastructures9070103.
[25] Y. Cheng, "Uncertainty propagation of flutter analysis for long-span bridges using probability density evolution method," *Reliab. Eng. Syst. Saf.*, vol. 251, 2024, doi: 10.1016/j.ress.2024.110361.